ENGINEERING SCIENCE AND TECHNOLOGY

Director's R&D Fund

Nanoscale, Explosive Energy-Burst Generators Using Controlled Nuclear-Mechanical Triggering of Pretensioned Liquids

R. P. Taleyarkhan,[1] C. D. West,[2] S. Hicks,[1] and J. S. Cho[3]
[1]*Engineering Science and Technology Division*
[2]*Physical Sciences Directorate (retd.)*
[3]*Oak Ridge Associated Universities*

This research focused on developing insights into a revolutionary class of explosive mechanical burst energy generators by tapping key physical attributes of pretensioned liquids which are fractured/triggered on the nanoscale (time and space) for explosive energy releases thereafter. Controlled triggering was achieved using neutron science technology in combination with pulsed lasers. The technology's potential was evaluated using theoretical analyses coupled with focused experimentation and was found to be promising. Estimates of energetics from experimental evidence indicate significantly larger quantities of energy-storage capability compared with conventional propellants. A table-top demonstration system was designed, fabricated, and tested.

Introduction

The goal of the project was to investigate the potential for energy storage in tensioned liquid metastable states followed by controlled release of the stored energy. The project workscope utilized neutron science, engineering expertise in acoustic studies for liquids and highly energetic materials, and life-science health effects assessment skills developed over the past several decades in various ORNL directorates.

It has been known for some time (although not widely recognized) that fluids, like solids, can be put under negative pressure (i.e., placed under tension). Upon reaching an appropriate state of instability, liquids can explode and release their stored energy. Such states can be reached via pretensioning or via suitable combination of pretension and thermal superheat. Experiments for determination of thresholds for fracture of pretensioned fluids under various states of treatment have been conducted[1] at ORNL and elsewhere.[2–7] The maximum possible extent of pretensioning prior to onset of cavitation for a properly prepared liquid such as water and mercury can be quite large and can reach close to -1400 bar (-20,000 psi) and -17,000 bar (-250,000 psi), respectively.[2–6] These tensile states are metastable and may be viewed for analogy as placing a spring under intense tension prior to snapping and explosive vaporization. The triggering of metastable fluids gives rise to explosive vaporization and release of stored energy which may be permitted to grow uncontrollably or induced to collapse to produce very high localized pressures and temperatures. This process, if conducted with suitable fluids, can possess the capability of producing enormous energy density (factors of 10^6 greater than that from CHNO compounds like TNT). Indeed, the controlled nuclear-based triggering of metastable fluids has recently been shown[8] by the authors to be capable of inducing nuclear fusion reactions between deuterium atoms during cavitation of deuterated acetone.

Technical Approach

The approach taken included the study and analysis of the literature on metastable fluid states induced via thermal superheat under positive pressure regimes and also by placing liquids under tension. The second phase of the project involved designing and fabricating a tensioned-metastability-inducing system to demonstrate nanoscale (space-time) triggering of the tensioned states in a variety of liquids with subsequent energy releases to propel an object.

Results and Accomplishments

A systematic study was undertaken to develop theoretical understanding of the various facets involved in energy storage during tensioned metastability and the nanoscale-to-macroscale triggering of energy bursts.

The nanoscale triggering of pretensioned liquids can be attained by subjecting individual nuclei of liquid molecules to knock-on collisions with energetic particles such as neutrons or the recoils from alpha particle decays. The collision of a high-energy (e.g., 14-MeV) neutron with an individual nucleus results in recoil-induced deposition of thermal energy in a nanometer-scale region of the targeted liquid. If this energy level is sufficient to cause a vapor nucleus to form with a radius larger than a certain

critical size of a vapor cavity, the cavity can then grow. Critical radii are usually in the nanometer range and are formed within nanoseconds. For example, for an organic liquid such as C_3H_6O, we calculate the critical radius to be about 28 nm with nucleation from dissolved alpha emitters or the knock-ons from energetic neutrons. Note that the extent (or quantity) of triggered formation of critical vapor pockets is dependent on the state of the fluid. The greater the pretensioned or metastable state, the lower is the initiation energy required. The closer the state is to that for homogeneous-explosive transformation, the larger will be the inherent, statistically induced fluctuations amenable to explosive vaporization. This will lower the initiation energy requirements. Figure 1 shows the experimentally determined variation of the normalized homogeneous or spontaneous-nucleation temperature with normalized pressure of the fluid field. Normalization is done relative to the critical point. Note that the data on which this plot is based involves extrapolation below the normalized pressure value of ~-1. This is based on the fact that the data above -l have been found experimentally[2,9] to follow a linear profile; therefore, the linear extrapolation into as yet uncharted territory is considered a reasonable initial engineering judgment. As will be noted, the greater the degree of pretension, the lower the stability limit and the easier it becomes to destabilize the entire system to explode. At a normalized negative pressure of -7 (i.e., -1400 bar) for water, the normalized temperature is only ~0.1 to 0.14 (i.e., ~30–50°C).

Triggering of explosive-burst generation can also be conducted via use of pulsed lasers. In this case, even if the metastable state is far from the stability limit, localized explosive-burst generation can be attained. Bulk triggering of metastable fluids can be attained via increasing the flux of incident neutrons, via use of laser (thermal) energy deposition, as also via use of acoustic energy that reduces the pressure to the limiting tensile state (as demonstrated for ether at ~120°C by Apfel[2] by reducing the pressure to ~–15 bar, at which point the conditions for system destabilization were met and the droplet exploded). As may be obvious by now, if the combination of pretension and temperature are at or close to the stability limits, bulk vaporization should be possible to initiate via intentional destabilization of a small region of the fluid space which propagates through the bulk fluid.

The means of storing energy in the fluid can be varied. The simplest device of storing and maintaining pretension is a centrifuge-type apparatus shown (for a specific configuration) in Fig. 2. The fluid to be explosively vaporized is placed in the central cavity, after which the centrifugal forces introduce the liquid to the desired degree of pretension. The degree of pretension will vary quadratically with the arm length of the centrifuge apparatus and rotation speed. As such, significant metastable states may be attained with a reasonable choice of parameters (e.g., -1000 bar with a length of 0.5 m and a spin rate of ~150 Hz). Other methods for introduction of metastable states in tension include acoustic means[2,7,8] and the Berthelot[3] method (with which the theoretical thresholds for pretension of water have been attained[6]). The use of acoustic means provides the capability to vary the frequency of tensile state attainment over a very wide range (e.g., up to tens of kHz). For our sonofusion studies,[8] we employed a chamber where ~15-bar (~250-psi) oscillating pressures were induced. We have also worked with multifrequency excitation[10] in which the transient pressure field can be composed of more than one pressure

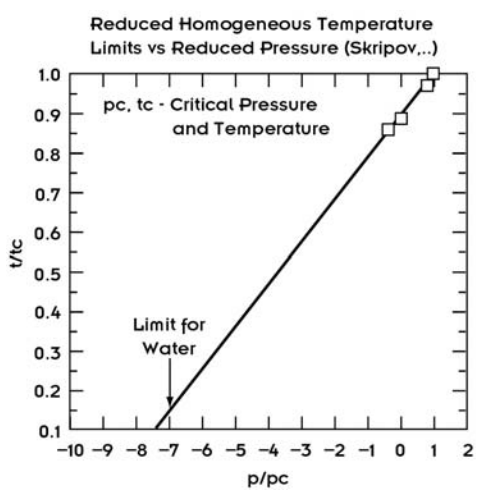

Fig. 1. Variation of normalized homogeneous nucleation temperature with normalized pressure (normalization done using critical state parameters).

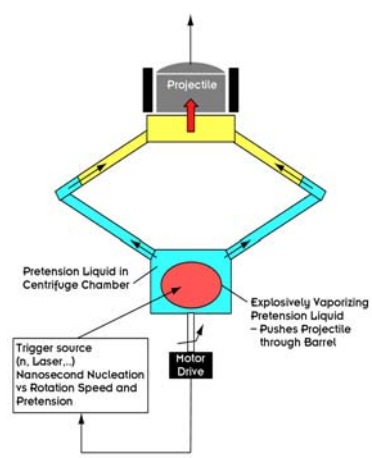

Fig. 2. Schematic arrangement of spinner experimental setup for determining energetics of Laser (nanosecond duration 0.3 mJ peak energy pulse) triggered explosive vaporization [arm length ~240 mm; liquid—acetone at 20°C; Radius of glass tubes ~2 mm (internal); Projectile mass ~0.5 g; Barrel length ~5 mm].

component. Such an acoustically excited system can possess the ability to store very large amounts of energy that can be released on demand (i.e., on triggering, which is something we have done successfully via pulsed-neutron-generator triggering). Transformation factors of output to input power have been observed experimentally by us to be in the several 10^3 range. The induction of extreme states of metastability requires careful preparation of the test liquid and its enclosure. Purity and degassing play an important role;[4,5] however, our studies indicate that prior precompression (to induce close-to-perfect wetting, and dissolve microbubbles) can play a far more effective role (as is clear when one analyzes the methods used and results obtained from tests by several experimenters[2,6]).

Energy is stored in a metastable fluid that, upon release in a controlled fashion, may then be used to deliver mechanical output to projectiles or surrounding structures. For pretensioned fluids, it is important to realize that the compressibility and specific heat capacity increase[11,12] as the degree of pretension increases, rising theoretically to infinity at the stability limit. Therefore, the amount of stored energy can become quite large, increasing nonlinearly with progressively enhanced states of metastability. An indirect method for estimating the work energy potential is to conduct experiments for bulk vaporization and localized explosive vaporization. Experiments[2] conducted with ether at ~120°C in an oscillating pressure field produced a relative volume change of ~10,000 to 20,000 (i.e., from liquid to vapor) over a millisecond of expansion. Conducting the calculation for *pdV*-type work, we estimated energy output of ~1–2 kJ/g of vaporizing material under positive pressure for conditions close to the limits of (thermal-superheat-induced) metastability. This is very significant when we realize that the work output from propellants such as nitrocellulose is only ~1.2 kJ/g.

An alternate experiment conducted involved introduction of metastable pretension in test liquids such as acetone, ethanol, etc., using a centrifugal system as shown in Fig. 2. As an example, for one case acetone was placed under pretension via spinning the apparatus to attain ~-5bar of negative pressure. Thereafter, a nanosecond timed laser pulse from a nitrogen laser caused explosive triggering at the focus point for a 1-mm-diameter region of the test liquid. The burst vaporization even at this relatively modest negative pressure (under room temperature conditions) resulted in the projectile being ejected at ~40 m/s (~150 fps) from which the *pdV* work output due to vaporization was estimated as ~0.6 to 0.7 kJ/g. While low compared to the ~1 kJ/g normally obtained from propellants such as nitrocellulose, it should be realized that this work output was obtained at only a small fraction of the theoretical pretension threshold. It is not known at present how the process will scale with various levels of metastability and other process parameters.

Summary and Conclusions

In summary, the combination of metastable states and appropriate triggering can offer the possibilities of nanoscale-to-macroscale triggering-induced explosive work output for a wide range of fluids. Various means ranging from centrifugal spinners to acoustic generators can be employed together with thermal management to induce desired states of metastability, which can then be destabilized explosively using nuclear to macroscale triggering techniques. The energy storage and work output potential from such releases can be significant and appear to be controllable. This promises to open up exciting possibilities in the fields of propulsion and possibly for nuclear fusion energy generation.

As a result of this project, the lead author was invited to present a keynote lecture entitled "Nano-to-Macroscale Triggering of Metastable Liquids"[13] at an international conference. We were also invited by the U.S. Army and several senior Pentagon officials (including the Vice-Chief of Staff Gen. J. Keane) to draft a white paper for planning the *Army of the Future* to potentially utilize this revolutionary technology. An invention disclosure was prepared and the technology was elected for filing with the U.S. Patent Office. An ORNL/TM report has been prepared.[14]

References

[1]R. P. Taleyarkhan and F. Moraga, *Nucl. Eng. Design* **27** (2001).

[2]R. Apfel, *Scientific American* **227**, 6 (1972).

[3]M. Berthelot, *Ann. De Chimie et de Physique*, Tome (XXX).

[4]L. Briggs, *Science* **109** (1949).

[5]M. Greenspan and C. Tscheig, *J. Res. Natl Bureau of Standards* **71C** (1967).

[6]Q. Zheng, D. J. Durben, and G. H. Wolf, *Science* **249** (1991).

[7]C. D. West and R. Howlett, *Acustica* **21** (1968).

[8]R. P. Taleyarkhan, C. D. West, J. S. Cho, R. T. Lahey, Jr., R. I. Nigmatulin, and R. C. Block, *Science* **295** (March 8, 2002).

[9]V. P. Skripov, *Metastable Liquids*, J. Wiley, New York (1974).

[10]F. Moraga, R. P. Taleyarkhan, R. T. Lahey, Jr., and F. J. Bonetto, *Phys. Rev. Lett.* **62** (2000).

[11]A. Hayward, *Nature* **202**(4931), 1964.

[12]R. J. Speedy, *Journal of Physical Chemistry* **86** (1982).

[13]R. P. Taleyarkhan, C. D. West, and J. S. Cho, *The Third International Conference on Transport Phenomena in Multiphase Systems (HEAT-2002), Kielce, Poland, June 24–27, 2002.*

[14]R. P. Taleyarkhan, C. D. West, and J. S. Cho, ORNL/TM-2022/233, November 2002.

Remote Emission Sensor Technology for Heavy-Duty Truck Emissions

R. N. McGill,[1] K. E. Lenox,[1] J. M. Storey,[1] A. Akerman,[1] C. W. Ayers,[1] H. D. Haynes,[1] T. Q. Dam,[1]
R. K. Richards,[1] S. Goedeke,[1] M. L. Simpson,[1] M.-D. Cheng,[2] E. A. Wachter,[3] and W. G. Fisher[3]
[1]*Engineering Science and Technology Division*
[2]*Environmental Sciences Division*
[3]*Galt Technologies, LLC*

The objective of this project is to develop low-cost, fast-responding, non-intrusive instrumentation for measuring certain emissions of heavy trucks as they pass on a highway. Prototype optical instrumentation has been developed for remotely measuring concentrations of nitrogen oxides (NO_x) and particulate matter (PM) in the exhaust plumes of heavy trucks. It is also important to acquire certain parameters about the truck's operating mode at the time emissions data are acquired. To this end, additional technologies were developed to analyze the acoustic signatures of trucks as they pass. From the acoustic signature, analysis data on the engine speed, turbine speed, and truck speed and acceleration can be developed. The three prototype instruments (including acoustic signature analysis software) have been tested against standard measures of exhaust species, and results compare favorably. They have also been validated in controlled, outdoor field tests using three different sizes of vehicles.

Introduction

Heavy-duty trucks account for large portions of the mobile-source NO_x and PM emissions in our urban environments, but truck emissions in the real world are not well characterized. It is difficult to attribute the emissions of a truck to its different modes of operation because truck engines, not the vehicles themselves, are certified for meeting emissions standards. In order to acquire large databases of in-use truck emissions, we must have access to emissions instruments that can acquire "snapshots" of a truck's emissions as it passes on a highway; that is, remote and non-intrusive instrumentation must be available. However, satisfactory instrumentation of that type has not been available to date. Therefore, to meet the need, this project has been focused on development of such instruments.

Technical Approach

We chose optical methods to achieve remote and non-intrusive measurements for NO_x and PM emissions. The NO_x instrument is based on an application of ultraviolet (UV) absorption, while the PM instrument is a greatly modified light distancing and ranging (LIDAR) approach. While these instruments are expected to yield concentrations of the pollutants in the exhaust plume of a truck, those measurements alone are not enough to characterize the emissions in terms of the truck's operation (e.g., grams per mile). To accomplish that goal we need a means to determine certain parameters of the truck's instantaneous operation, such as speed, acceleration, weight, engine speed, and turbine speed. It was thought that these parameters could be deciphered from the acoustic signature of a passing truck. Therefore, the third leg of the project is to develop acoustic signature analysis instrumentation that will provide data on the truck's operating parameters, including engine and turbine speeds, as the truck passes on the road. The technical approaches for each of these three technologies are discussed individually below. In all three cases, the development took similar courses. Bench-scale experiments were first used to test and improve the methodologies. After methodologies were confirmed, experiments moved to the engine laboratory scale, using real engines to generate the exhaust. At the last stage of development, all three instruments were tested in a chassis dynamometer laboratory with a vehicle generating the exhaust. Included in this last stage of development were outdoor tests with selected vehicles moving past the measurement station.

UV Absorption for NO_x Measurement

A double-pass UV instrument was developed for the measurement of nitric oxide (NO) concentrations. A deuterium lamp was used as the UV source to provide a broad continuum. The light from the lamp was directed with quartz optics into an approximately parallel beam from the instrument. This beam was directed through the region to a mirror—a UV-enhanced retro reflector—that returned the light beam back to the UV instrument. The returning light was focused into a spectrometer (HR2000, Ocean Optics) that measured its spectrum from 200 to

300 nm. A laptop computer controlled both the spectrometer and the data using a USB serial line.

Data from the spectrometer were collected and analyzed using software developed with Visual Basic version 6.0. The determination of the NO concentrations was made by first measuring the spectral intensity under conditions without NO present. This provided a reference intensity level. Measurements were then made with NO present, and the differences used to determine the spectral absorption. The NO concentration was determined using the strength of the absorption lines around 226 nm. The spectral background between 220 and 230 nm was used to estimate broadband absorptions and scattering losses due to water vapor, unburned fuel, rain, dust, etc. After correcting for theses other losses of light, the remaining absorption feature around 226 nm was fit to a multiple line shape, which then provided the absorption due to nitric oxide. The 226-nm wavelength was selected because it had no interference from sulfur dioxide or ammonia absorption.[1]

This instrument was calibrated using a 1.6-m cell set in the path of the light beam between the instrument and the retro reflector. A gas flow was maintained through the cell at 1 atmosphere of pressure using a combination of the chemical to be analyzed and nitrogen. A gas mixer was used to adjust the concentration of the chemical under study. The chemicals studied in this way included NO, sulfur dioxide, and ammonia.

Most of the calibration effort involved the study of NO. The concentrations of NO were varied between 0.5 to 1000 parts per million (ppm). The results were fit with a third-order polynomial to determine the concentration based on absorption strengths. The results were found to be reproducible to within approximately 2% with long measurement times (~10 s). Such a long integration time would not be practical for the measurement of effluents from passing vehicles, so the accuracy as a function of integration was examined. For short time periods, the inaccuracies grew as the inverse square root of the integration time. For an integration time of 50 ms, the results were found to be reproducible to within approximately 10%.

FM-CBR LIDAR for PM Measurement

The challenges of measuring a diffuse target, such as truck PM exhaust, require the ability to monitor rapidly varying particulate concentration profiles that can be very small compared to the ambient concentration profiles. Using the superior noise suppression provided by phase-sensitive detection enables the use of low-power, eye-safe, inexpensive light sources such as diode lasers. To achieve these goals, we have developed a hybrid modulation scheme called frequency-modulated coherent-burst ranging (FM-CBR). This combines key aspects of traditional LIDAR systems to achieve sensitive, precise measurement of the distance and concentration of diffuse targets at data bandwidths exceeding 1 kHz. This measurement technique is a variation of CBR, which was first developed at ORNL.

FM-CBR LIDAR uses an interrupted series of high-frequency amplitude modulation pulses encoded on an optical carrier. The use of high modulation frequencies, combined with high data acquisition rates, allows several positions in a passing exhaust plume to be monitored in quick succession. The system is monostatic (i.e. the laser and light collector are all on the same axis), which greatly simplifies alignment without a significant sacrifice of signal (Fig. 1). The laser used is a widely available red laser diode (632 nm) combined with a frequency matched photomultiplier tube for light collection.[2,3,4]

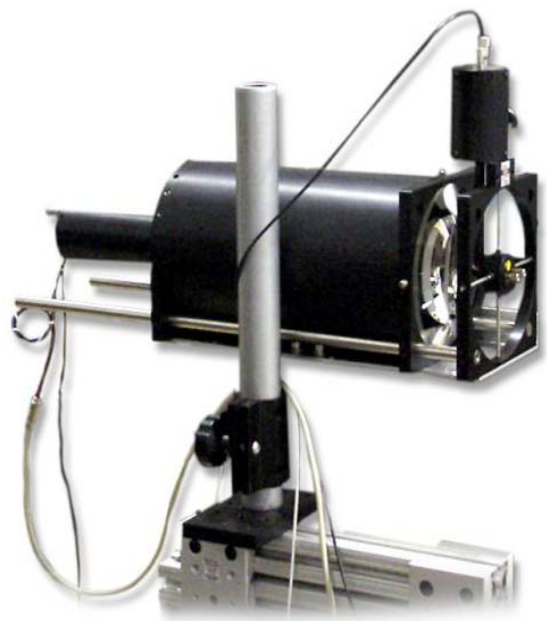

Fig. 1. Monostatic LIDAR system for measuring PM emission concentrations.

Acoustic Signature Analysis for Acquiring Engine Operating Parameters

The challenge in deciphering a sound recording of a passing truck is to efficiently extract the desired information from the sound. In theory it should be possible to determine the truck's engine and turbine speeds from the acoustic signature. These data, together with knowledge of the typical size of a heavy-duty truck engine, will allow the estimation of the exhaust flow rate at the time of the measurement. Knowing the exhaust flow rate, the emissions concentrations from the instruments developed in this project, and the speed and acceleration of the truck, we should be able to closely estimate the emissions of NO_x and PM on a grams-per-mile basis.

Results and Accomplishments

UV Results for NO_x

The goals of this aspect of the project were met with a demonstration of the instrument's capability for measuring several chemicals (NO, sulfur dioxide, and ammonia) and the measurement of NO concentration from the exhaust from a diesel engine. The diesel exhaust measurements were performed with both a stationary vehicle on a dynamometer (see Fig. 2 for results) and with several passing vehicles. Note that the measurement results are in ppm · m since the light beam integrates through the cloud of effluent. For the investigation of the passing vehicle, three vehicles were tested; a Mercedes A Class, a Ford F-250, and a Peterbilt heavy-duty truck tractor. The Peterbilt was also tested on a street location in Chattanooga, Tennessee. Example results from these tests are illustrated in Fig. 3 showing the NO concentration from the Ford F-250.

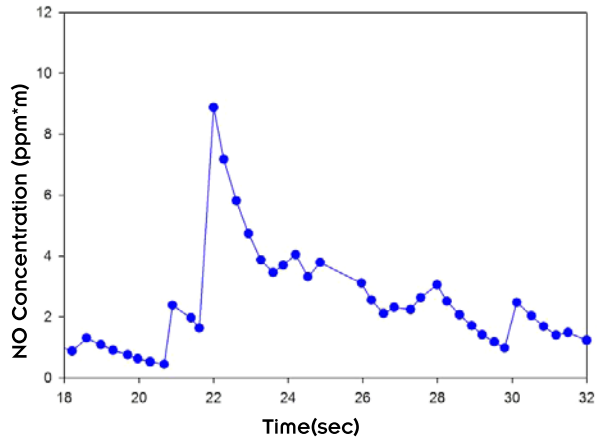

Fig. 3. Measurements of NO concentration from a Ford F-250 diesel passing through the optical beam at approximately 22 seconds. Although the data integration time was 50 ms, the data analysis required several hundred milliseconds yielding only a few data points per second.

FM-CBR LIDAR Results for PM

To confirm that the range and resolution of the LIDAR system were sufficient to meet the measurement goals, a series of experiments were performed using "hard" targets, such as clear sheets of plastic and Delrin®, a highly reflective material. This initial work provided the information needed to refine the hardware and software in order to proceed onto more challenging measurements. After successful completion of these experiments, the focus of the experiments became the investigation of the ability of the LIDAR system to detect particle sizes and size distributions. Thus we moved from hard targets to laboratory-generated aerosols.

In general, aerosols interact with laser light in three ways: they absorb the light, they scatter the light forward, and they scatter the light backward. By knowing the aerosol particle-size distribution, the wavelength of the laser light, and the effective refractive index of the particles, one can derive a theoretical volume backscatter coefficient, β, analogous to the reflectivity of a surface, using Mie theory.[5] The amount of light scattered backward from an aerosol plume can then be calculated from this coefficient. Thus β is the common link between LIDAR measurements and microphysics models of aerosols. As a first step in validating our instrument, experiments were performed with known aerosols, and the measured value of β from the LIDAR measurements was compared to that from Mie theory.

We had mixed results from our experiments with laboratory aerosols. In all cases, the data clearly show a difference between two aerosols and the location of the aerosol streams, the signal to noise ratio is good, and the results are repeatable. Typical results with the "hard" targets and with a highly reflective aerosol are illustrated in Fig. 4.

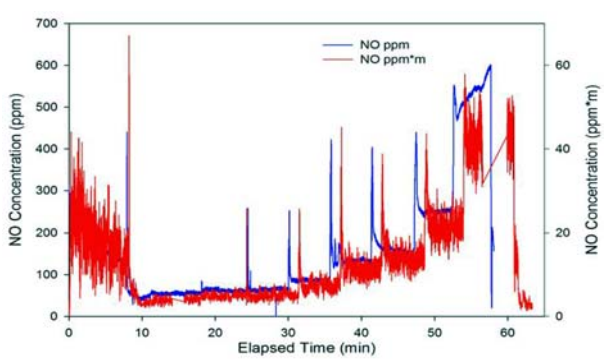

Fig. 2. Comparison of NO measurement techniques. The blue curve is from the heated chemiluminescent detector taking samples in the exhaust tail pipe and the red curve from the UV absorption instrument measuring the concentrations 40 cm after the tail pipe.

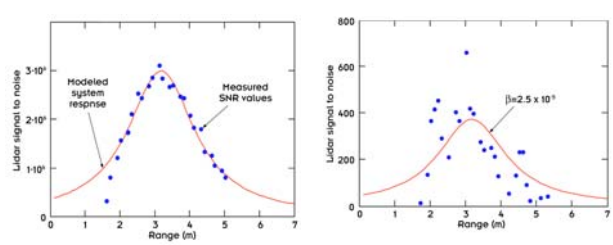

Fig. 4. The measured and modeled FM-CBR LIDAR system response to a hard target made of Delrin (on the left) and a laboratory generated aerosol of ammonium sulfate. Note that the scatter has increased dramatically for the aerosol. However, in the aerosol case the calculated beta value of 2.5E–6 does agree favorably with the theoretical value of 3.23E–6.

The experimental focus moved to real exhaust measurements—first in a chassis lab and then in an outdoors setting. FM-CBR LIDAR and scanning mobility particle sizer (SMPS) measurements were taken of the exhaust of a light-duty diesel vehicle on a chassis dynamometer operating at a range of steady-state conditions. The FM-CBR measurements were repeated with the same vehicle driving by in a parking lot at speeds up to 40 mph. Similar measurements were taken using a full-size diesel truck and a heavy-duty diesel tractor. For the outdoor experiments, no data existed to make a β value comparison, so the signal-to-noise ratio was used to compare the data. The high signal-to-noise ratios, as shown in Fig. 5, indicate that the location and presence of the exhaust plume are being detected by the FM-CBR system.

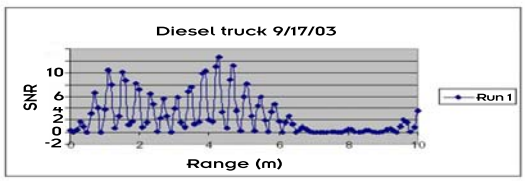

Fig. 5. The FM-CBR system response to exhaust from a moving vehicle.

It is the correlation between backscatter and particle size and distribution that needs refinement.

Acoustic Signature Analysis for Acquiring Parameters of Engine Operation

A typical fast Fourier transform (FFT) shows little or no signal at the fundamental engine speed, but as one would expect, significant harmonics, including strong 3rd and 6th harmonics are present. From this there is sufficient information to determine the engine speed from the acoustic signature. In addition we have identified the signature sound from the turbocharger in the acoustic data. A part of the turbocharger spectrum is shown in Fig. 6. This is a waterfall plot to demonstrate the change in frequency of the turbocharger as the truck goes up a slight grade maintaining a constant engine speed (rpm).

Many techniques have been developed for analysis of time-series data such as a sound signature. We have employed linear techniques to date. Using a method that looks for discrete spectral components, we have written programs in LabView that automatically analyze a data set for engine speed and show the turbocharger frequency as a function of time.

One version of this is shown in Fig. 7. On the left side are two data sets showing signals from trucks going uphill on I-40 at Lovell Road, Knoxville, Tennessee. Subsequent traces are superimposed so that the change in frequency of the turbocharger signal may be clearly seen. Unless the truck is using engine braking, the turbocharger signal is absent when the truck is going downhill. A third program called Truck Acoustic Data Analyzer (TADA) combines these with additional analysis tools that provide an indication of engine load in nearly automatic fashion.

Another consideration in the development of the acoustic signature analysis techniques is the need for the most efficient methods for collecting data along the highway unattended. A two-channel broadband microphone and amplifier was constructed and used for much of our collection, indicating a clear pathway to an unattended system.

Each of the three technology developments included in this project has advanced the body of knowledge in their respective fields. Invention disclosures are being prepared for both the FM-CBR LIDAR technology and the acoustic signature analysis technology. The researchers have produced a number of technical papers and presentations thus far, and we anticipate more of such in the near future. The high-frequency amplitude modulation of the FM-CBR LIDAR along with the phase-sensitive lock-in detection of signal has produced a unique system with large signal-to-noise ratio and capable of rendering the particulate concentration in the beam path in a manner

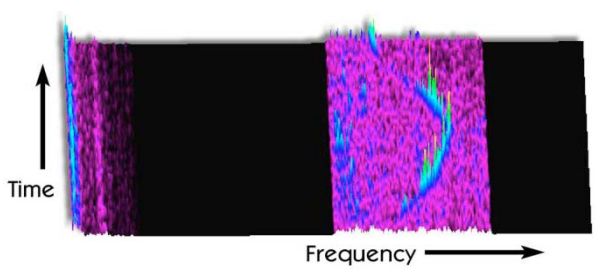

Fig. 6. A "waterfall" plot of engine and turbine speeds as a truck goes up a hill. Engine speed (to the left) remains relatively constant as the truck maintains a constant speed. But, turbine speed (to the right) first increases, as the truck requires more power to go up the hill at constant speed, then decreases as the truck crests the hill.

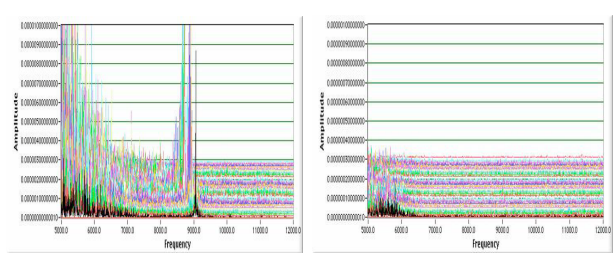

Fig. 7. The change in frequency shown in subsequent traces on the uphill (left side) charts is due to the Doppler shift as the truck passes the microphone. The downhill trucks (right side) do not show the turbocharger peaks.

that has not heretofore been accomplished. This technology promises to be applicable in a number of other scenarios including the issues of homeland security. The advances in the field of acoustic signature analysis represented in this project have a number of potential commercial applications relative to vehicle/engine diagnosis and maintenance as well as the intended use in this project in remote sensing of truck operations.

Summary and Conclusions

Working prototypes have been produced for the three different instruments to measure remotely the NO_x and PM emissions and engine operating parameters of passing trucks. Novel technologies have been employed, and patent disclosures have been filed for two of the technologies. Our goal of low-cost instruments has been achieved; all three technologies can be fabricated at much lower cost than typical instruments of a similar type. Validations of the operations of the instruments have been performed in real-world settings. More work is needed to "harden" the instruments for use alongside a road and to automate their processes to produce real-time results of measurements.

These developments will benefit DOE, EPA, and the Federal Highway Administration (FHWA) as they attempt to gain a better understanding and characterization of in-use emissions from heavy-duty trucks. Data are sorely needed to characterize the heavy trucking sector's role in urban air quality problems, and these instruments will help to clarify the effects.

This project has been part of a larger vision for an ORNL role in studying truck emissions and their impact on local environment. That vision is captured in the Watt Road Environmental Laboratory Initiative (WRELI). Knox County, Tennessee, is funding the University of Tennessee and ORNL to monitor emissions at one of the large truck travel centers at the Watt Road interchange, and discussions continue with the FHWA to fund a similar but larger project to study the emissions inventory along the roadbed of I-40. Efforts to further develop the WRELI vision, and the technologies of the project will continue.

References

[1]T. E. Barber, J. Castro, S. Hnatyshyn, N. L. Ayala, J. M. E. Storey, and W. P. Partridge, "Analysis of Diesel Engine Exhaust by Ultraviolet Absorption Spectroscopy," *Analytical Letters* **34**(14), 2493–2506 (2001).

[2]E. A. Wachter and W. G. Fisher, "Coherent Burst Laser Ranging: Decoupling Resolution and Unambiguous Range," *Opt. Lett*. **22**, 570 (1997) .

[3]E. A. Wachter and W. G. Fisher, "Method and Apparatus for Coherent Burst Ranging," U.S. patent 5,745,437.

[4]E. A. Wachter and W. G. Fisher, "Method and apparatus for improved ranging," U.S. Patent 5,889,490.

[5]H. C. Van de Hulst, *Light Scattering by Small Particles*, Wiley New York, 1957.

Nanoscale Photonic Crystal Laser

J. T. Simpson,[1] M. L. Simpson,[1] S. Rajic,[1] P. G. Datskos,[1] G. E. Jellison,[2] C. W. White,[2] and S. P. Withrow[2]
[1]*Engineering Science and Technology Division*
[2]*Condensed Matter Sciences Division*

The goal of this project was to demonstrate the first silicon nanocrystal waveguide–based laser (i.e., to show stimulated emission from a high-"Q" resonant cavity using silicon nanocrystals as the cavity's optical gain medium). Before we achieved our main goal of showing stimulated emission, a number of smaller goals had to be met. We demonstrated the ability to form silicon nanocrystals in SiO_2 by ion implantation and for ultraviolet light to generate silicon-nanocrystal-based photoluminescence. We then demonstrated the ability to form a matrix of high-Q distributive-feedback structures, each of which contained a large concentration of silicon nanocrystals. And finally we demonstrated the ability to optically pump these structures in order to generate stimulated emission. This project has been a multifaceted research effort involving not only ORNL but also Lawrence Livermore National Laboratory, the University of Arizona, and Digital Optics Corporation.

Introduction

Integration of optical components within semiconductor microchips has been a goal for many years. Such integration could create new and improved devices. The main reason why this integration has not occurred is the lack of any small CMOS compatible laser sources. Current solid-state lasers generally use gain media of non-standard III-V (or II-VI) materials, such as GaAlAs formed in a multiple quantum-well configuration. Such non-standard materials are difficult to fabricate and are highly incompatible with standard semiconductor microchip processes, which are generally silicon based. A solid-state laser suitable for integration with standard semiconductor microchip processes would be constructed from silicon-based materials, or at least be CMOS compatible, and would include a semiconductor process compatible optical waveguide material to facilitate energy transport. However, several challenges, including the indirect bandgap characteristic of bulk silicon, have generally prevented fabrication of silicon-based lasers. In 2000 Pavesi et al.[1] showed that silicon nanocrystals (embedded in a silicon dioxide matrix) produced an intense photoluminescence when optically pumped with ultraviolet light. Further investigation by Pavesi's group and others[2–6] showed the ability of such nanocrystals to act as an optical gain media with gains reported as high as 100 cm^{-1}. This project combines the recently discovered optical gain of silicon nanocrystals in the near IR region of the spectrum with an ORNL-designed, high-Q, distributive feedback (DFB) optical-waveguide structure. When optically pumped, using a high-intensity pulsed ultraviolet laser, this structure showed stimulated emission at 835 nm, thus demonstrating the world's first silicon nanocrystal waveguide–based laser. This groundbreaking research project enables the integration of micro-optics and opto-electronics with semiconductor microchips. Such integration is enabling to a host of optical technologies including optical interconnects, new types of chemical and biological sensors, new types of optical waveguide-based modulators, and is a vital component for optical computing.

Technical Approach

The goals of this research were to model, design, simulate, fabricate, and characterize the world's first silicon-nanocrystal-waveguide laser. To accomplish these goals, it quickly became apparent that multiple research and development paths were required. We began with two parallel paths of effort. The first path involved the creation of photoluminescent silicon nanocrystals, while the second path was to model, design, and computer simulate a high-Q DFB waveguide resonant cavity structure. While the ion implantation team worked on perfecting the implantation of the silicon and the formation of silicon nanocrystals, the resonant cavity design team worked on the design, modeling, and simulation of the DFB resonant structure. The ion implantation team used ORNL's ion

implantation facility to establish the best recipe for silicon nanocrystal creation. Once the ion implantation group had the right recipe for making silicon nanocrystals and the resonant cavity design team had a good cavity design, the two paths merged into the integration and fabrication phase of the project. During this phase, both groups worked together and began collaborating with other research and fabrication groups at the Lawrence Livermore National Laboratory (LLNL), the University of Arizona's Optical Sciences Center, and Digital Optics Corporation in Charlotte, North Carolina.

Initially we planned to do all the waveguide cavity fabrication and optical measurements at ORNL, but, based on our simulations and subsequent design choices, it soon became apparent that we required state-of-the-art photolithography equipment and expertise. This necessitated the photolithography work going outside the Laboratory. LLNL researchers assisted us in both high-quality optical thin film deposition and in e-beam photolithography. Some of the modeling and simulation problems and results were discussed with faculty and graduate students from the University of Arizona. We also subcontracted with Digital Optics Corporation to fabricate a two-dimensional array of DFB structures using state-of-the-art deep ultraviolet photolithography using I-line steppers. We also took advantage of their optical processing expertise with silicon dioxide to etch and dice some of the fabricated devices.The testing and characterization phase was primarily performed at ORNL.

Results and Accomplishments

Silicon nanocrystals: The ion implantation steps were performed at ORNL. A number of different ion implantation recipes, consisting of differing concentrations of silicon atoms, annealing temperatures, annealing durations, implantation energies, and substrates were tried and evaluated. The recipe that produced the largest photoluminescent characteristics (i.e., the brightest emission when pumped with ultraviolet light) is the one we used with our high-Q DFB cavity design and is described as follows: Multiple ion implantation energies were used to obtain a relatively uniform (flat) concentration profile of 5×10^{21} atoms/cm^3 throughout the top 500 nm of the substrate. The matrix substrate material used was fused silica. The samples were annealed for 1 h at a temperature of 1100°C. Annealing at this temperature caused significant migration of the excess silicon atoms. This migration had three distinct advantages. This large silicon migration allowed surface damage from the ion implantation to be repaired. Migration also caused the coalescence of silicon atoms into nanocrystals and increased the uniformity of the resulting effective index of refraction profile. The resulting nanocrystals have an estimated mean diameter of approximately 3 nm.

Planar waveguide: The index of refraction of fused silica is known to be 1.45 for near-infrared wavelengths. When fused silica contains silicon nanocrystals with a concentration of 5×10^{21} atoms/cm^3, the resulting index of refraction is increased to at least 1.55. We took advantage of this increase in refractive index and the uniformity of its profile to form a planar waveguide within the top portion of the fused silica substrate. Next, a thin film (approximately 1.0 µm thick) of SiO_2 was deposited (by chemical vapor deposition) on the planar waveguide's top surface. This allowed the planar waveguide to have a semi-symmetric structure which significantly enhanced the waveguide's modal characteristics. Figure 1 shows our fabricated planar waveguide and the photoluminescence observed when the sample was illuminated by a 1-W CW laser having a wavelength of 413 nm. Note how intense the photoluminescence appears in the image. Figure 2 shows the measured photoluminescence spectra from the sample seen in Fig. 1. Note that most of the emission from this sample is in the near-infrared regime, while only a small amount emits in the visible. Thus most of the emission can't be seen by eye or CCD camera. This makes the CCD generated image in Fig. 1 that much more impressive.

Modeling, Design, and Simulation: Modeling and simulation was performed using two commercially available sets of modeling software. The first software package we used, GSOLVER,[7] allowed us to establish an initial design for the cavity. Unfortunately, GSOLVER ran very fast by making a lot of simplifying, and sometimes unrealistic, assumptions. The algorithm GSOLGER uses

Fig. 1. CCD Image of the silicon nanocrystal photoluminescence from a 0.5-µm layer of silicon nanoparticles in a 2-cm-diameter SiO_2 wafer. Excited with 413-nm, 1-W CW laser.

what is known as "rigorous coupled wave equation" analysis. The second software package, FIMMWAVE[8] ran much slower, using algorithms based on much more complicated but more realistic assumptions. FIMMWAVE uses algorithms based on "modal analysis." We based our final design on simulations using this modal analysis package. A series of different waveguide cavity designs were modeled and simulated. The one chosen to be

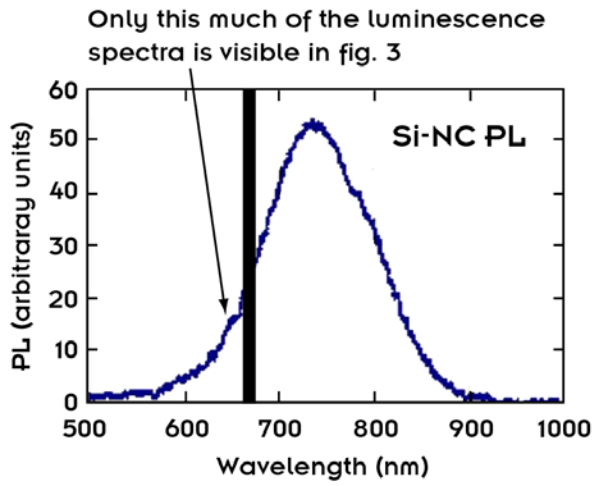

Fig. 2. Spectral response of the photoluminescence from a 0.5-µm layer of silicon nanoparticles in a 2-cm-diameter SiO_2 wafer. Excited with 413-nm, 1-W CW laser. Measured with an Ocean Optics spectrum analyzer.

implemented was a channel waveguide DFB. This design was chosen for its fabrication simplicity, superior performance characteristics, and its ability to be fabricated from the planar waveguide provided by our ion implantation team members. Because all the etching was on the overcoat layer and didn't directly affect the channel waveguide core region, this design was very insensitive to small processing defects. Any periodicity defects simply shifted the resonant wavelength slightly while any defects in the etch depth or uniformity simply reduced the resonant Q slightly. The design called for a 1-mm^2 channel to be etched into the silicon nanocrystal planar waveguide. Within this channel, 4000 shallow (500-nm-deep) grating periods were to be etched. Each period was to be one-half of an optical wavelength in extent. Assuming the waveguide's effective index of refraction was 1.55, the required periodicity turned out to be 250 nm. The theoretical Q of this design was roughly 100,000. Such a high Q means that virtually all of the stimulated emission generated within the structure will leak out of plane before coming out the ends. This extremely high Q was much greater than needed and made greatly relaxed the fabrication processing tolerances required. Figure 3 shows a simplified (much smaller number of periods) channel waveguide DFB structure schematic, and Fig. 4 shows its associated simulation results when formed into a resonant cavity having a quarter wave offset in its center. Since the silicon nanocrystals showed maximum photoluminescence at a wavelength of 750 nm, this was chosen to be the design wavelength for our cavity.

Fabrication: Our design called for forming a channel waveguide and distributive-feedback (DFB) structure via photolithography and chemical etching. Even though our DFB design was substantially easier to fabricate than most other designs investigated, it is still very difficult due to the small dimensions (250-nm periodicity) and the associated tight tolerances required (±5 nm). These fabrication issues led us to collaborate with Digital Optics Corporation in Charlotte, North Carolina. With their help we were able to come up with a fabrication strategy to successfully form such a channel waveguide having a DFB structure with 4000 periods. They also suggested we create a two-dimensional array of such structures using their state-of-the-art I-line photolithography steppers. Each channel

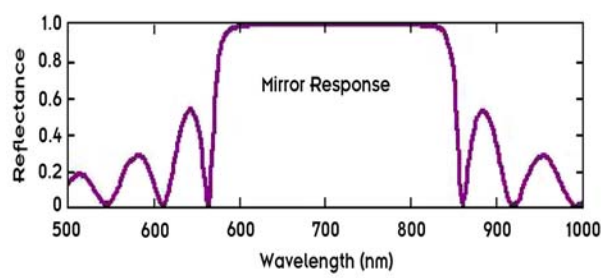

Fig. 3. Simulated spectral response of a distributed feedback (mirror) structure having a periodicity of 250.

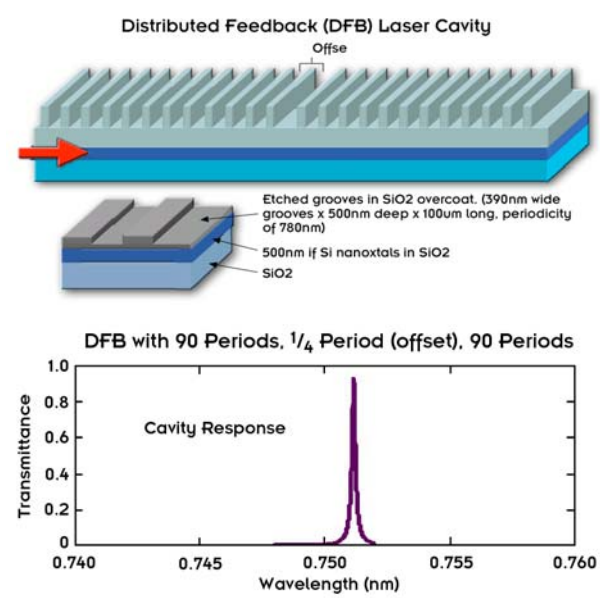

Fig. 4. Schematic and simulated spectral response of a distributed feedback (cavity) structure having a periodicity of 250 nm.

waveguide DFB structure was fabricated to be slightly different (i.e., slight differences in grating periodicities and line widths). This was accomplished by varying the optical focus and or the exposure dosage as the stepper imaged different channel waveguide DFB structures on different areas of the wafer. The result is known as a focus-exposure matrix, which is a fabrication development technique to help optimize fabrication processing parameters. Figure 5 shows an optical interference image of a fabricated DFB offset region and alignment mark. The distortion seen in the image is due to distortion in the imaging system and not the fabricated part. The etching line widths and parallelism design tolerances were all met according to the SEM and AFM measurements. Figure 6 shows an atomic force microscope (AFM) image of part of the DFB structure created. Figure 7 shows an image of many channel waveguide DFB regions making up a focus-exposure matrix of structures.

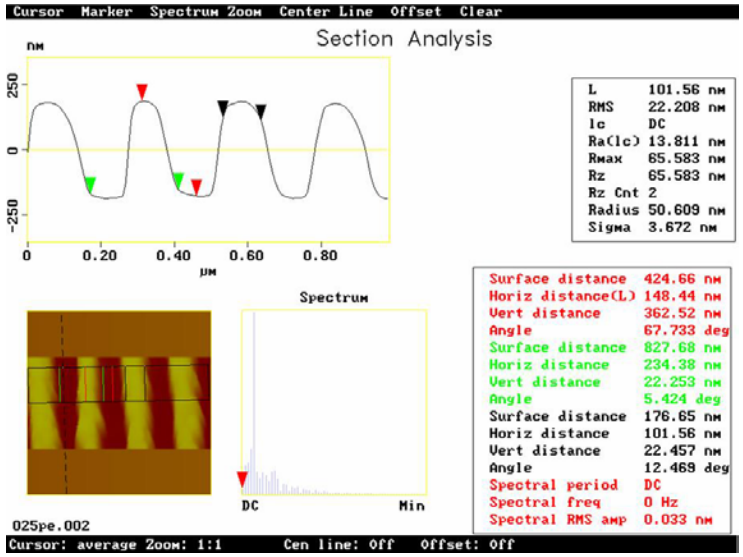

Fig. 6. Atomic force microscope image of a distributed feedback structure with a periodicity of 250 nm.

Testing and Characterizations

Once we completed fabrication of the focus-exposure matrix of channel waveguide DFB structures, we began the testing and characterization phase of the project. We used a pulsed 337-nm wavelength nitrogen laser having pulse durations of 800 ps and pulse outputs of 2.8 µJ to optically pump our structures. The nitrogen laser emitted a rectangular beam approximately 3 mm × 10 mm in extent. This beam was focused down to approximately 1 mm × 3 mm. This allowed us to illuminate a single channel waveguide structure at a time. Again, since the Q of the structures was so high, we expected most of the emission to leak out the top rather than come out the ends. As expected, we saw virtually no emission out the sides. But, as expected, we saw a large leakage emission coming out the top surface. Figure 8 shows the spectral emission of this leakage. While he had expected emission to be at 750 nm, you can see from Fig. 8 that it actually emitted at 835 nm. Most likely this discrepancy is due to an underestimation of the effective index of refraction of the channel waveguide. The 845-nm emission suggests that the actual channel waveguide index of refraction is 1.75 instead of 1.55.

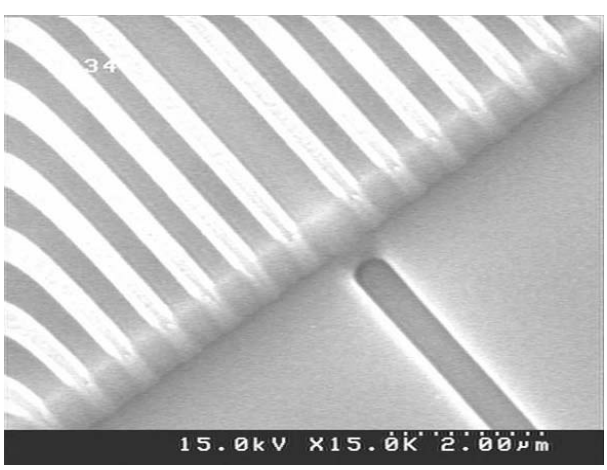

Fig. 5. Optical interference image showing the fabricated distributed feedback offset region and alignment mark. The apparent distortion is due to limitations in the optical imaging system.

Summary and Conclusions

In order to achieve the ultimate goal of this project of demonstrating silicon based stimulated emission, many intermediate goals and accomplishments had to be met. First and foremost, we had to form photoluminescent silicon nanocrystals. We then had to use these photoluminescent nanocrystals to form a planar waveguide within a SiO_2 substrate. Finally we measured the spectral emission observed when the channel-waveguide distributive feedback (DFB) structure was optically pumped using a pulsed nitrogen laser. A broad spectral photoluminescent emission is produced by the silicon nanocrystals being pumped by ultraviolet laser light, while a narrow spectral emission is observed which is caused by stimulated emission generated within the channel-waveguide DFB structure. This observed stimulated emission was our research goal and as such demonstrates

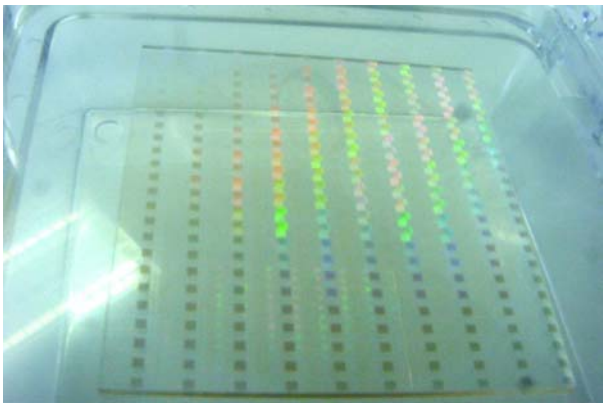

Fig. 7. Image of a glass slide patterned with a distributive feedback focus-exposure matrix.

the world's first silicon nanocrystals–based waveguide laser. Another major accomplishment of this research has been the collaborative effort involving two national labs (ORNL and LLNL), a major university (the University of Arizona's Optical Sciences Center), and an industrial partner (Digital Optics Corporation). This research has demonstrated the ability of silicon nanocrystals to be used as a gain media in conjunction with a high-Q distributive feedback structure. This groundbreaking research project enables the integration of micro-optics and opto-electronics with semiconductor microchips. Such integration is enabling to a host of optical technologies including optical interconnects, new types of chemical and biological sensors, and new types of optical waveguide-based modulators and is a vital component for optical computing. We are in the process of submitting these results for peer review and publication. Now that stimulated emission has been demonstrated using silicon nanocrystals, we are pursuing sponsorship to expand the scope of this research, which would include the possibility of electronically pumping the silicon nanocrystals and combining the silicon nanocrystals with erbium. We already have some follow-on DARPA funding to explore the silicon nanocrystals with erbium combination.

References

[1]Pavesi et al., "Optical gain in silicon nanocrystals," *Nature* **408**, 440 (2000).

[2]Khriachtchev et al., "Optical Gain in Si/SiO2 Lattice: Experimental Evidence with Nanosecond Pulses," *Appl. Phys. Lett*. **79**, 1249 (2001).

[3]Ivanda and C. W. White, "Stimulated Emission and Optical Gain in Silicon Nanocrystals," *Applied Physics Letters,* 2031–33 (2000).

[4]Degoli et al., "Electronic and Optical Properties of Silicon Nanocrystals: Structural Effects," *Mat. Res. Soc. Sym. Proc.* **770**, I1.9 (2003).

[5]M. A. Green et al., "Exceptionally High Radiative Efficiencies in Silicon," *Mat. Res. Soc. Sym. Proc.* **770**, I2.7.1 (2003).

[6]L. Dal Negro et al., "Time-resolved Gain Dynamics in Silicon Nanocrystals," *Mat. Res. Soc. Sym. Proc.* **770**, I3.4.1 (2003).

[7]*GSOLVE*R from the Grading design software from Grating Solver development Company of Allen, Texas.

[8]*FIMMWAVE and FIMMPROP-3D* custom waveguide design software from Photon Design, Inc., of Oxford, United Kingdom.

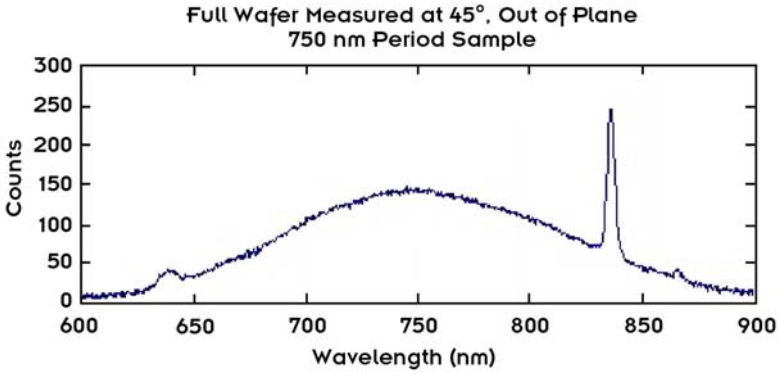

Fig. 8. Spectral emission showing a broad photoluminescent emission and a narrow distributive feedback structure emission at 835 nm.

Zero-Power, Low-Cost Sensor Platform

J. E. Hardy,[1] P. D. Ewing,[1] J. E. Christian,[1] R. J. Warmack,[1] P. G. Datskos,[1] C. L. Britton, Jr.,[1]
M. Z. Martin,[2] and S. F. Smith[1]
[1]*Engineering Science and Technology Division*
[2]*Environmental Sciences Division*

Numerous national studies and working groups have identified very low-power, low-cost sensors as a critical technology for increasing energy efficiency, reducing waste, and optimizing processes. This research will address that need by developing a zero-power, low-cost sensor platform based on microcantilever (MC) arrays that includes MC sensors, very low-power electronics, signal processing, and two-way data communications, all integrated into a robust package. MCs will be developed to measure carbon dioxide, temperature, and room occupancy. Research areas are coatings for the various gases, developing an electronic readout for the infrared occupancy sensor, and developing very low power readout and signal transmission (both over power lines and wirelessly).

The objectives of this research effort is the development a near zero-power, low-cost platform based on a microelectromechanical-system (MEMS) sensing array. This sensor platform will include microcantilever (MC) sensors, very low-power electronics, signal processing and filtering, and data transceivers all integrated into a robust package. The vision is to develop a flexible multisensor array (measuring several items concurrently) that will use little to no net power, be very low cost in volume (<$100/unit), and communicate bidirectionally either over existing power lines or wirelessly. The focus of this project is to develop MEMS sensors to be able to eventually monitor a variety of gases, temperature, and personnel occupancy that are important in many applications. The R&D required to achieve the proposed vision includes the development of coatings for the cantilever array and the development of low-power signal processing and communications electronics. State-of-the-art improvements will be needed in multisensor array/electronics integration, conversion of infrared sensing to a very low-power electronic readout (instead of optical), and low-power data transmission/coupling to existing power lines. Success in this proof-of-principle effort will enable us to obtain a leadership role in DOE programs related to energy efficiency/waste reduction [e.g., zero-energy buildings (ZEB), fossil energy, fuel cells, distributed energy resources].

The microsensor array prototype will be based on ORNL inventions in MCs, low-power electronics, and sensor networks. Coatings will be developed based on literature review and our polymer experience, the infrared (IR) occupancy sensor will be an extension of previous work in IR imaging with MCs, the electronics will be based on several years of experience in low-power design and integration, and the sensor network will be based on our inventions in hybrid spread-spectrum communications.

During the first year of the project, we developed a chemical coating that is sensitive to carbon dioxide, has reasonable response times, and is relatively stable with minor influences from humidity. We also successfully tested a ten-channel capacitive readout and signal conditioning electronic module. The electronics are very low power (1 mW in continuous use and microwatts in intermittent use) and have very low noise levels (equivalent to a nanometer of movement in the MC). We made good progress in the design and fabrication of infrared MCs that can be read out electronically (first of its kind) and completed conceptual design for a robust communication scheme that uses existing building wiring and can handle three-phase noise. An invention disclosure was filed on this robust communication scheme.

This project is relevant to DOE in several mission areas including building technologies, industrial technologies—sensors and controls, and fossil and fuel cell energy technologies. The zero-power, low-cost sensor platform will allow more extensive monitoring of building processes and environmental conditions for personnel health and comfort. The research into low-power electronics and multisensor arrays will advance measurement science—an enabling technology for most DOE programs. This project has applications to Department of Defense programs and Homeland Security programs. The low cost of our platform should allow more and better monitoring of ships, tanks, and planes, which will increase in importance as manpower is reduced in the armed forces. The low power and low cost allows more monitoring and detection for security needs. In addition, the zero net power enables sensing in remote locations, giving unattended monitoring—a must for security and homeland defense.

NEUTROMEGAS: A Pixel Detector for Neutron Imaging

C. L. Britton, Jr.,[1] W. L. Bryan,[1] A. Wintenberg,[1] R. J. Warmack,[1] T. E. McKnight,[1] S. Frank,[1]
R. G. Cooper,[2] N. Dudney,[3] and G. Veith[3]
[1]*Engineering Science & Technology Division*
[2]*Spallation Neutron Source (SNS)*
[3]*Condensed Matter Sciences Division*

A bright neutron source such as the Spallation Neutron Source (SNS) places extreme requirements on detectors and especially impacts a detector's imaging and dynamic range. Present imaging detectors have either shown position resolutions that are less than acceptable or they exhibit excessive paralyzing dead times due to the brightness of the source. A new detector concept known as MICROMEGAS (MICROMEsh GAseous Structure) has been developed at CERN in Geneva for high-energy charged-particle tracking and has shown great promise for handling high data rates with a rather low-cost structure. If properly developed, this detector platform has features that could revolutionize neutron imaging. We are presently developing a novel detector using the MICROMEGAS concept by creating NEUTROMEGAS, the first pixelated, high-rate detector for 2-D neutron imaging. This has not been successfully accomplished anywhere else, although it has been a goal for researchers. This would be an outstanding contribution to the overall detector instrumentation effort for the neutron community and would establish ORNL as a leader in the development of next-generation neutron detectors.

Objective

The goal of this project is to develop a prototype high-(position) resolution, low-dead-time neutron detector that we call NeutroMegas. In order to accomplish our goals two key projects have been undertaken. One focuses on the development of the detector structure and readout electronics, while the other is directed towards converter foil research. The detector structure portion of this project will entail building and testing both one-dimensional (1-D) strip and two-dimensional (2-D) pixel detectors. Initially a 1-D strip prototype will be developed since it allows easy electronics readouts, while our long-term goals will be to produce a true pixelated 2-D detector

During the first year of the project, we fabricated a detector prototype whose anode structure was formed on a quartz substrate using micro-fabrication techniques. A regular array of separator columns 73 µm tall was formed by chemically etching the photopatterned surface. A shadow mask was then aligned to permit 250-µm-wide chromium anode strips to be evaporated between the columns. Adjacent strips were spaced 1 mm apart and were alternately connected to vacuum feedthroughs in the aluminum chamber. A 1000-line-per-inch, 7-µm-thick nickel grid was placed atop the anode structure. A 3-mm insulator was then used to space a boron- or lithium-coated aluminum converter plate away from the grid.

The main objective of the neutron converter work has been to develop the synthetic techniques required to fabricate the converter foils as well as understanding and manipulating the chemical or electrochemical stability of these foils. This is essential to successfully building a stable, high-efficiency detector. To this end, we have been very successful in meeting our goals.

Converter films consisting of naturally abundant elements have been prepared using a variety of physical deposition techniques. Due to the air and moisture sensitivity of these materials, all film growths were carried out in a deposition system contained within an argon-filled dry box. Thin films of boron (1–2 µm) and gadolinium (1–2 µm) have been prepared using RF and DC sputtering techniques, respectively, while lithium films (3–100 µm) were synthesized by thermally evaporating elemental lithium. These thickness ranges were chosen from the literature for reasonable detector efficiency. The deposition conditions were optimized (i.e., argon pressure, power, distances between the targets and substrates, rate and choice of substrates) in order to minimize the film impurities as well as reduce any potential mixing of the reactants due to the energetic nature of the deposition process. By optimizing the deposition conditions, we have effectively reduced the impurity content to below 5 atomic %.

In summary, we have established the synthetic conditions required to prepare these foils, investigated a series of Li-substrate interactions, initiated a series of long-term studies to address the interdiffusion between the converter constituents, and determined the stability of the converter to the detector gases.

Because the detector has worked so well in a short period of time, we have had opportunity to do extensive testing. Our testing includes the following:

1. *Critical Voltage (E_{crit}) testing*—The critical voltage E_{crit} is the voltage when electron multiplication begins for a given gas and detector geometry. Calculations for our geometry at 1 atm of P-10 gas predicted a value of E_{crit} = 350 V for our multiplying grid voltage. Our measurements showed a value of approximately 330 V, demonstrating excellent agreement with the design value.
2. *Detector position mapping with ^{241}Am*—With the data acquisition system (DAQ) we developed, we can simultaneously read out each of the six instrumented channels of strips in two different modes. The observed position-sensitive detector spectrum is exactly what we expected to see with this detector and data system.
3. *^{252}Cf Testing (neutron testing)*—Mode 2 of the DAQ allows us to stop and read all channels any time one of the strips has an event. This allows position determination of an incident neutron in 1-D, the very purpose of the detector. We have been able to observe individual neutron events with little crosstalk between strips.

At the end of the second year of this project, we expect to have a working 2-D pixel detector. This should attract interest from instrument scientists at the SNS for use in beam and transmission monitoring applications in some of the proposed experiments. In addition, a variant of this detector is being considered by another experiment at SNS.